



Article submitted to journal

Subject Areas:

astrophysics, stars, spectroscopy

Keywords:

Solar corona, magnetic activity,
elemental abundances, solar cycle,
solar-stellar connection

Author for correspondence:

David H. Brooks

e-mail: dhbrooks.work@gmail.com

Evolution of solar and stellar coronal abundances due to magnetic activity

David H. Brooks^{1,2,3}, Deborah Baker²,
David M. Long³, Paola Testa⁴
and Harry P. Warren⁵

¹Computational Physics, Inc., Springfield, VA 22151, USA

²University College London, Mullard Space Science Laboratory, Holmbury St. Mary, Dorking, Surrey, RH5 6NT, UK

³National Institutes of Natural Sciences, National Astronomical Observatory of Japan, 2-21-1 Osawa, Mitaka, Tokyo, 181-8588, Japan

⁴Centre for Astrophysics & Relativity, School of Physical Sciences, Dublin City University, Glasnevin, D09 K2WA, Dublin, Ireland

⁵Harvard-Smithsonian Center for Astrophysics, 60 Garden St, Cambridge, MA 02193, USA

⁶Space Science Division, Naval Research Laboratory, Washington, DC 20375, USA

We discuss the evolution of solar coronal element abundances over an active region lifetime. Magneto-convection drives the complexity of magnetic fields that emerge above the photosphere. This complexity is dissipated, together with that of the overlying pre-existing fields, through dynamic events such as flares. A period of stable "ordinary" coronal heating ensues, before the concentrated fields are dissipated through interactions with the surrounding environment. The evolution of coronal abundances can be explained by the First Ionisation Potential (FIP) effect operating within this framework. We extend the discussion from magnetic activity on timescales of active region lifetimes (months), to the solar cycle (years), and stellar evolution (eons). The broad picture shows intriguing similarities that may prompt new investigations.

1. Introduction

The First Ionization Potential (FIP) effect is now established as an increase in the abundance of low FIP elements (such as Fe, Mg, Si) in the solar corona compared to the photosphere, while the high FIP elements (such as Ne and O) retain their photospheric abundances or are slightly depleted. The boundary between low- and high-FIP elements is usually observed to be around 10 eV. The effect was originally noted from spectroscopic observations of the solar corona during rocket flights in the 1960s [1], and was later detected in the solar wind, solar energetic particles (SEP), and galactic cosmic ray sources [2]. The effect is thought to operate in the chromosphere where there are many potential ionizing processes. H I Ly α radiation is dominant, however, and the transition energy of 10.2 eV is close to the observed boundary between low- and high-FIP elements. It therefore ionizes the low FIP elements only and creates a separated reservoir of ions and neutrals. A mechanism is then needed to preferentially transport the ions to the corona, that is likely intimately linked to the coronal heating process itself, and leads to an observed fractionation of elements in the corona.

A promising possibility is the ponderomotive force (PF) arising from propagating Alfvén waves. These may be generated in the convection zone [3] or produced by magnetic reconnection [4,5]. Alfvén waves propagating downward from the corona reflect and refract after impinging on the chromosphere from above. The associated upward ponderomotive force transports ions to the corona. Different fractionation scenarios that modulate the magnitude of the FIP effect and/or the behaviour of different element ratios result from whether the waves are resonant on closed field structures or non-resonant on open field [6,7]. This is potentially useful for understanding compositional differences between the fast solar wind, that is thought to originate in open field regions such as coronal holes where non-resonant waves are pervasive, and the slow solar wind that may originate in coronal loops. Recent observational evidence supports both the idea of a role for wave activity in FIP fractionation [8,9] and the existence of wave reflection in the chromosphere [10]. The chromosphere is, of course, a complex and dynamic environment. Recent multi-fluid magnetohydrodynamic (MHD) simulations including collisional coupling and the effects of wave damping suggest that ponderomotive acceleration could occur in the direction of wave propagation [11]. Further work is needed to fully understand the FIP effect in realistic dynamic solar conditions.

Another aspect of the FIP effect that has generated recent interest is the detection of the inverse-FIP (iFIP) effect on the Sun [12] during flares. An inverse effect was first observed on RS CVn-type binary stars [13,14] and some very active K-dwarfs [15]. Subsequent observations found that M-dwarfs also show an iFIP effect [16]. Some doubts about the initial observations were founded on the uncertainties associated with the photospheric abundances of solar-like stars, but further independent support has come from the detection of the iFIP effect in localized regions of strong magnetic field, such as sunspots or sunspot light bridges, during solar flares [12,17]. The iFIP effect has also now been detected in the slow solar wind [18].

A key question is whether the iFIP effect is a unique clue to the workings of the coronal heating mechanism, or whether the FIP and iFIP effects are just different aspects of the same basic process. The models of the FIP effect we have referred to here [4,11] both invoke the ponderomotive force acting preferentially on the low FIP ions with the iFIP effect arising from the direction of the ponderomotive force, which is related to the direction of Alfvén wave propagation in these models. For example, if fast mode waves generated by subchromospheric reconnection are propagating up from below, the ponderomotive force will be directed downwards in one of the models [4]. There is now some observational evidence that both effects work on the low FIP elements. The detection of the iFIP effect in the slow solar wind using particle counting techniques indicated a depletion of the low FIP element Fe [18], while the extended cooling times of iFIP patches in post-flare coronal loops suggests reduced radiative losses also indicative of low FIP element depletion [19]. The same conclusion was earlier drawn from measurements of column depths in iFIP locations [20]. Of course, the observations are complex and contradictory, and in

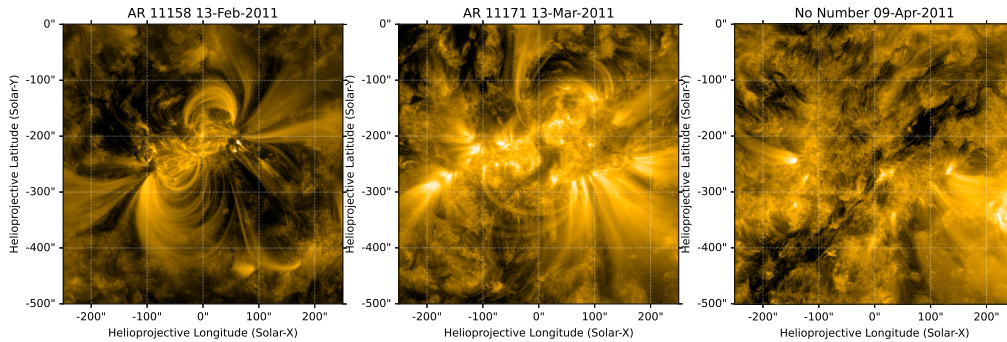


Figure 1. SDO/AIA 171 Å images of the evolution of AR 11158/11171 as it passes the central meridian on three rotations. The magnetically complex, dynamic, and compact structure of emerging AR 11158 develops into the larger, diffuse, non-flaring AR 11171, and finally devolves into a filament channel before dissipation in the quiet Sun.

theory the iFIP effect could be a distinct process enhancing neutrals. There is also evidence that the FIP effect is caused by the depletion of high FIP elements in some stellar coronae [21].

These developments highlight the complexity of the FIP and iFIP effects arising potentially from the direction of wave propagation (upward/downward), and resulting in disparate behaviour (enhancement/depletion) in different elements (low and high FIP). Nonetheless, the recent observations and theoretical work suggest that *the overarching process is simply the depletion of low FIP elements from the chromosphere* with the different observed (FIP/iFIP) effects resulting from the opposite direction of diffusion. Future theoretical work will pin down whether the depletion is *in the direction of the wave source* (e.g. coronal or sub-chromospheric reconnection), or *in the direction of wave propagation* (e.g. aligned with spicules).

In light of this background, we review the known results on the evolution of coronal abundances in active regions (ARs), and develop a picture of the changes due to magnetic activity. In this paper, when we refer to AR coronal loops, we are referring to what we observe in EUV and/or soft X-ray images of the solar corona: a narrow emission feature where we can observe the footpoints and the apex. There is some evidence that observed loops are composed of much finer threads that are below the resolving power of current instrumentation, but this is a question that has not been settled [22–24]. Following the description of AR evolution, we extend the discussion to solar cycle timescales, and the solar-stellar connection.

2. Coronal abundance evolution in active regions

While our description of the evolution of coronal abundances in ARs is intended to be general, we refer to one widely studied region (AR 11158) to aid the discussion. To observe all the features in such an AR comprehensively throughout its lifetime is challenging with the limited field-of-view (FOV) spectrometers that can measure plasma composition. Nevertheless, here we assume that the activity in this AR is broadly illustrative of a typical AR lifetime and can be related to the spectroscopic properties measured in other ARs.

AR 11158 emerged around 2011 February 10, and is shown Figure 1 after substantial growth on February 13. This region produced multiple flares and coronal mass ejections and has been the subject of intensive studies [25–28]. The AR grows rapidly from $\beta \rightarrow \beta\gamma \rightarrow \beta\gamma\delta$ Hale class producing an M6.6 flare a couple of days after emergence, and reaches a total area in excess of $3.04 \times 10^{19} \text{ cm}^2$ and total unsigned magnetic flux of at least $4.22 \times 10^{21} \text{ Mx}$ as early as February 12 [29]. The region was observed as it tracked across the disk, and then again on the second rotation as AR 11171, and the subsequent rotation as an unnumbered diffusing active area. Figure 1 shows images of the AR as it crosses the central meridian on the three rotations. AR 11158 emerged into a relatively quiet environment - although there is some interaction with AR 11156

to the solar west - and initially consisted of two bipoles before developing into a highly complex region with four sunspots and strong shearing of the neutral line. Such magnetic complexity, driven by magnetoconvection below the surface, always leads to significant flare activity as the magnetic stresses are relaxed. AR 11158 produced one X-class, 7 M-class, and 66 C-class flares according to the Hinode Flare Catalog [30]. Activity reduced to a single M1.5 flare as AR 11171 on the second rotation, and no flares on the third rotation.

Hinode/EUV Imaging Spectrometer (EIS) [31] data for this region show that the emission measure distribution is peaked near 3.5MK in its early emergence phase, but that the slopes above and below the peak are shallower than found in magnetically stronger ARs, suggesting relatively lower frequency heating in the core [29]. This is presumably because it was observed by EIS while still in the emergence phase, when it was clearing the surrounding environment and its own magnetic complexity. Lower frequency heating in the core at this time is in agreement with observations of high variability at the footpoints of hot core loops in other ARs [32–34]. Observations have also shown that the peak temperature decreases and enhanced cool and hot emission below and above the temperature peak dissipates with time as ARs age i.e. the heating frequency in the AR core increases [35].

If a magnetically simple and stable AR emerges into a quiescent environment, the AR corona will be heated through processes that might be described as "ordinary" coronal heating. Of course the actual heating mechanism is unknown, but if we adopt the definition, discussed earlier, of a coronal loop as a distinct feature in an EUV image that is composed of a number of sub-resolution magnetic threads [23,24], then examples of these processes might include internal reconnection of braided threads within the loops, such as occurs in nanoflares [36] or in an MHD avalanche [37,38], or alternatively, high frequency Alfvén wave turbulence heating [39], or chromospheric jets supplying mass and energy and forming loop structures [40–43]. The idea is that a specific *internal* heating process will occur within the AR loops, and this will naturally occur if the AR evolution is undisturbed by the pre-existing surrounding magnetic environment.

Conversely, if the AR and pre-existing magnetic environment is highly complex, then the AR evolution will first be affected by *external* reconnection with pre-existing fields, dissipation of emerging twisted magnetic fields, and/or large scale field misalignments [44,45]. This dissipation of magnetic complexity in the early phase by flares and flare-like intermediate processes [44,45] ultimately dominates the initial AR evolution, and delays the AR from settling down to the ordinary coronal heating phase seen in magnetically simpler ARs. Eventually the AR region field weakens and starts to interact with surrounding quiet Sun fields. This might lead to similar signatures as observed in the early phase, albeit of less dramatic magnitudes, for example, small-scale impulsive heating events rather than larger scale flaring events. Magnetically complex ARs can thus pass through three broad phases:

- Emergence - dominated by external processes that remove complexity (reconnection with pre-existing field, dissipation of twist)
- Stable - dominated by internal processes (ordinary coronal heating)
- Dissipation - competition between internal processes (ordinary coronal heating) and external interactions (with the surrounding magnetic environment).

With this picture in mind, the elemental abundances that we measure should reflect a transition from a complex field external reconnection based development to an internal heating mechanism controlled development. Here we review what plasma composition measurements we might expect to make, and what we actually observe.

During the early emergence phase one would expect to see photospheric or weakly fractionated abundances indicative of emerging flux [46], essentially reflecting the composition of the quiet corona [47]. When flares are dominant, we see a wide variety of results depending on flare-class, flare-phase, and elements measured. Large flares lead to the evaporation of photospheric material, at least at 10 MK [48], though measurements show spatial variations from photospheric to coronal abundances in features such as post-flare loops [49]. Coronal material has

also been found in the flare decay phase in X-ray spectra [50,51]. A recent paper gives a summary of many of the flare composition results in its Appendix [52]. Close to the strong magnetic fields of sunspots we may also see the iFIP effect. We also see a large amount of impulsive heating events on a smaller scale in the transition region. They are predominantly clustered around the neutral line where large flares are also expected [53]. These events also show a photospheric composition [54]. The key point is that at this time a whole range of large and small-scale flaring composition signatures are competing to dilute the characteristic abundances of the AR in its stable phase. When the external reconnection has stopped, the AR quickly forms a very typical structure, with a hot core (3–4 MK) above the moss at the footpoints of high temperature loops, peripheral high lying warm (2 MK) loops, and bright fan loops (1 MK) at the AR edges intermixed with high temperature outflows that have been connected with the solar wind [55–57]. On the subject of the outflows, they also form quickly and again there are arguments that this is an external reconnection induced development. Observations of one AR showed that within hours the typical AR structure was established with the reconfiguration of the magnetic field that formed the outflows apparently initiated by a small CME (coronal mass ejection) [58]. Interchange reconnection [59,60] between closed and open field at the AR boundary is a popular explanation for the formation of the outflows. In EIS observations, the predominant abundance diagnostic uses Si and S lines [61,62], and the outflows show a strong FIP effect [62,63].

The closed magnetic field structures in the AR core also show a strong FIP effect in measurements using the same Si/S diagnostic [29]. The underlying moss would be expected to reflect a similar composition, though there is also some evidence of mixing due to dynamic events [63–65]. Warm loops are assumed to show coronal abundances, but there are relatively few good measurements of these loops. In EIS observations, the presumed coronal abundance leads to relatively weak S emission, which makes measurements difficult. The bright fan loops certainly show a strong FIP effect [54,66].

This then is the basic compositional structure of ARs. As they age, however, further changes occur. Studies from Skylab initially indicated that the FIP bias (ratio of coronal to photospheric abundances) increases [67] but this does not seem to be observed clearly with EIS. EIS observations have shown that the regions dissipate through interactions with the surrounding environment, including eruptive activity [46,68].

Considering this perspective on this typical AR evolution, one could ask what we would see in an averaged AR spectrum rather than in spatially resolved features. The Skylab results found in the early phase of the ARs evolution, when we expect flares to occur, could be understood in that we would measure emerging flux with a photospheric composition, and this flux reconnects with pre-existing field to cause flaring, some fraction of which also produces photospheric composition. This photospheric composition might obscure the appearance of the coronal composition signature associated with the AR emerging in the quiet Sun until all the complexity has gone and the AR has moved to a stable phase driven by ordinary coronal heating. In this scenario it is not so much that the FIP bias is increasing, but that we initially observe the dominance of structures and events that have a photospheric FIP bias, and later we then observe the structures that have a coronal composition dominating. This dominance of coronal composition plasma then increases as the AR grows and develops with more and more of the AR encompassing the surrounding area. Finally, there would be a reversed phase at the end of the AR lifetime as the region dissipates, although observations of such dissipating ARs are rare. To be clear, the emergence→stable→dissipation cycle we discuss above would manifest in the composition measurements as dominated by photospheric (emerging flux/flares)→coronal (AR)→mixed (dissipated AR/quiet Sun).

3. Coronal abundance evolution over the solar cycle

If our picture of elemental abundance changes associated with AR evolution is close to being correct, it naturally leads us to consider what we would see on solar cycle timescales. Elemental abundances in the solar wind are known to show variations with the solar cycle [70–74]. The high

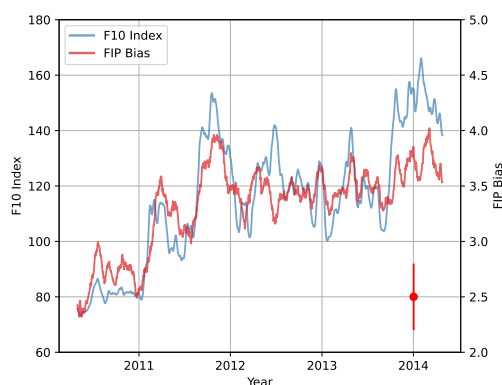


Figure 2. Temporal evolution of the full disk integrated F10.7 cm radio flux (blue) and the FIP bias (red) between April 2010 and May 2014. The data are 27-day Carrington rotation running averages. The FIP bias is measured by computing the full disk temperature distribution (DEM) using spectral lines of the low FIP elements (Mg, Si, Fe) observed by SDO/EVE and modelling the intensity of a strong line from the high FIP element Ne. The ratio of predicted to observed intensity yields the FIP bias. This plot is an adaptation of Figure 2 from Brooks et al. (2017) [69] and their error estimate is plotted as the red vertical bar.

FIP element He, for example, increases in abundance at solar maximum in the slow wind [71]. An important question is whether this reflects cyclic variations in the source regions, or only reveals itself in the solar wind after acceleration. Evidence from coronal streamer and Sun-as-a-star observations suggests the former explanation [69,75]. Figure 2 shows the variation of FIP bias and F10.7 cm (2.8 GHz) radio flux during the rise phase of solar cycle 24 from April 2010 to May 2014. The FIP bias measurements are from the Extreme ultraviolet Variability Experiment (EVE) on SDO and reflect the variation of the coronal abundances of the low FIP elements Fe, Mg, and Si, compared to the high FIP element Ne. The FIP bias is strongly correlated with the F10.7 cm radio flux during the rising phase ($r = 0.9$), though it appears to saturate at solar maximum. One uncertainty is that the result is based on the high FIP element Ne, and the O/Ne ratio shows a similar increase at solar maximum in the solar wind [74]. This behaviour could reflect the lower FIP of O relative to Ne, or could be due to a depletion of Ne. The issue is discussed further in the original paper [69].

This solar cyclic dependence of full disk integrated coronal abundances is broadly explained by the contribution of ARs (and other features) to the averaged spectrum. At solar minimum, there are few if any ARs, and a typical quiet Sun coronal composition is measured. In Figure 2 it is 2.3, though the F10.7 cm radio flux has already risen above the absolute solar minimum value, so if the correlation holds throughout the solar cycle the FIP bias may go lower. This will also depend on the abundance diagnostic used. EIS Si/S and Fe/S measurements suggest a value closer to 1.4 or 1.5 [76], though this is influenced by the behaviour of S, which fractionates differently in different circumstances [6]. In fact EIS spatially resolved observations of the full Sun allow us to disentangle the contributions of quiet features and ARs to the measured FIP bias of 1.4. In specific observations from January 2013 [77], the area coverage of ARs with FIP bias in the range 2–4 is $\sim 28\%$. The mean value when combined with the $\sim 72\%$ coverage of features with an average FIP bias ~ 1 is close to 1.4. In that context the EVE results look a little high. This could reflect the different elements used, but the calculation is also different. The FIP bias comes from full disk average spectra, so it is the contribution of the spectral line intensities rather than the area coverage that matters. Consider, for example, the EIS observations of the strong Fe XII 195.119 Å line. A typical value in the quiet Sun is $\sim 135 \text{ erg cm}^{-2} \text{ s}^{-1}$ [78], whereas it was measured as $\sim 2729 \text{ erg cm}^{-2} \text{ s}^{-1}$ in AR 11158 [29]. For an EVE observation with ARs like AR 11158 covering 30% of the area of the disk the ARs contribute 90% of the total intensity of the spectrum.

During the rise phase of the cycle, the area coverage of ARs increases and their contribution to the full disk integrated measurement consequently increases. In this phase, the ARs are isolated and magnetically simple. They emerge with a photospheric or weakly fractionated composition, but this signature would be hard to detect in the full Sun data even if there were several ARs on disk. Since they are magnetically simple and are emerging into a less magnetically complex environment, they proceed to the ordinary (internally driven) coronal heating phase relatively quickly and develop a coronal composition. This signature is seen in the rise of the FIP bias with the cycle, and it increases as ARs of larger magnetic flux appear and as the area coverage increases.

As we approach solar maximum, more complex ARs appear, but their composition signatures now include the initial phase where their complexity is dissipated by external processes inducing large flares and impulsive events that evaporate photospheric, or even iFIP effect, plasma. They develop a strong FIP effect as they transition to the ordinary coronal heating phase, but the overall competition between the signatures of many ARs at different stages of their evolution leads in part to the saturation of FIP bias observed in Figure 2. This also manifests itself as a non-linear component in the FIP bias-F10.7 cm radio flux correlation at high levels of solar activity, which can be seen as the separation of the curves in Figure 2 around 2014.

Another reason we observe the non-linear component during increased magnetic activity is that there is a tendency for gyroresonance emission to increase its contribution to the radio flux when there are larger, stronger magnetic concentrations, whereas the FIP bias tends to be lower above sunspots than it is in more evolved ARs [79]. It may be that a clearer linear correlation could be observed by comparing the FIP bias with the total unsigned magnetic flux with the sunspot contribution removed, but this has not been attempted yet. Large equatorial coronal holes that form at solar maximum also complicate the picture. EIS observations indicate that at least some equatorial coronal holes show a FIP effect [77].

4. Coronal abundance evolution of the Sun in time

There have been extensive studies of solar-like stars that have attempted to relate FIP bias measurements in stellar coronae to properties of the stars. Some of these investigations have revealed a dependence on spectral type, suggesting a relationship with fixed properties such as rotation rate and/or surface temperature [80]. It is clear that there is also some dependence on activity level as measured by, for example, the X-ray to bolometric luminosity ratio [81].

If we relate our discussion of the solar cyclic FIP bias effect (based on our discussion of AR composition evolution) to the development of solar-like stars on stellar evolutionary time-scales, we might expect a relationship between FIP bias magnitude and stellar age, and this has been investigated in the past [85]. This would be the case if the coronae of magnetically complex and active stars were analogous to the Sun's corona at the peak of the solar cycle phase, and if the coronae of more evolved and less active stars were analogous to the Sun's corona at solar minimum. Of course, such comparisons are difficult to make due to the number of variables involved: different stellar classes are not necessarily comparable, stellar masses, rotation rates, metallicities etc. are different. In fact, it is not the case: young highly active stars show a strong iFIP effect that dominates their coronae. We can see examples of this in Figure 3, which shows the FIP bias as a function of age for a sample of magnetically active stars [82]. This study explored the dependence of the FIP bias on many of the stellar properties (surface gravity, metallicity, age, Rossby number etc.) while prioritising homogeneity in the parameters in the sample. They also attempted to address the significant uncertainty in similar studies that results from adopting solar photospheric abundances in the FIP bias calculation by using (or in some cases measuring) the stellar photospheric abundance. From their results reproduced in Figure 3, we can see that flaring M-dwarf stars, and some K-dwarfs, especially fast rotators, show a strong iFIP effect. Most of these stars have estimated ages of < 2 Gyr. In contrast, A-F and solar type stars show a normal coronal FIP bias or close to photospheric abundances. Stars older than 3 Gyr show a solar-like FIP effect.

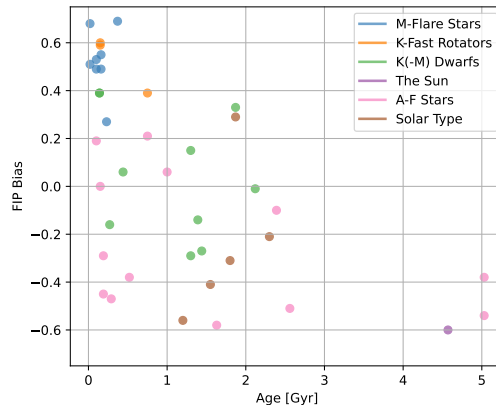


Figure 3. FIP bias against stellar age for a sample of magnetically active stars [82]. We plot a subset of the original literature sample excluding evolved RS CVn-type stars, those with undetermined ages, and Proxima Centauri. The definitions of the stellar type in the legend are taken from Table 1 in the original paper. The ages and FIP bias values are taken from Table 2. We use the "literature" FIP bias values, which are derived from measurements of the coronal to photospheric ratio of the mean abundances of some combination of C, N, O, and Ne relative to Fe i.e. $[X/Fe] = \log[X/Fe]_{cor} - \log[X/Fe]_{phot}$. This definition means values of $[-0.5, 0, 0.5]$ correspond to a solar FIP bias of $[0.32, 1, 3.2]$. The active Sun appears at 4.57 Gyr. Stellar measurements of photospheric abundances were used when available, but otherwise solar photospheric abundances from [83] and [84] for Ne were used. The specific values are given in Table A.1 of the Appendix of the paper [82].

The evolutionary change could be from an iFIP effect to a solar-like FIP effect [85]. This can be understood within our discussion framework. We know from solar observations that the iFIP effect occurs in magnetically complex ARs and so far has only been seen in high temperature emission during solar flares. It has also been associated with e.g. subchromospheric reconnection [86]. Stars that show an iFIP effect, therefore, may have coronae with emission dominated by highly complex ARs that can produce iFIP effect plasma. External reconnection processes such as flare reconnection, or subsurface interactions of sunspots, are known to occur in such complex ARs. We should recognize, however, that once this complexity is cleared on evolutionary timescales (i.e. the magnetic activity of the star has decreased), the corona should come to be dominated by ARs in their ordinary, stable (internally driven) coronal heating phase, or indeed somewhat more magnetically simple ARs such as are seen in the early rise phase of the solar cycle. Basically, stars with an iFIP effect corona should move directly from the top left to the lower half of Figure 3 without passing through a phase of photospheric dominance, regardless of their later evolution. Stars with coronal emission dominated by photospheric abundances could just be at the minimum phase of their cycles, or all activity may have ceased, or they may never have developed a FIP effect in their coronae if their chromospheres are relatively inactive [80,87].

5. Discussion

We have attempted to draw together connections between observations of coronal abundance evolution over a solar ARs lifetime, the solar cycle, and stellar evolution timescales. We put forward an overview of the influence of magnetic activity on coronal composition on these timescales. It is clear, however, that there are fundamental complexities that we have necessarily simplified.

At a basic level, all of the elemental abundance measurements are founded on EUV and X-ray spectroscopic techniques that are built on a number of assumptions. The differential emission measure (DEM) analysis that underpins the measurements has long been a source

of controversy and there is a view that the techniques are fundamentally limited [88–90]. It is easy to generate conflicting abundance results using different DEM methods even when the underlying observational and atomic data are basically the same. Furthermore, in these evolving magnetic environments the impact of plasma dynamic effects such as non-equilibrium ionization, non-Maxwellian electron distributions, collisional disruption of dielectronic recombination and ionisation, can all play a role. An integrated study of the competition and influence of these effects on abundance measurements still awaits.

Accepting the results as they are, we see systematic differences dependent on the species used in the analysis. We mentioned the behaviour of elements such as S that lie close to the boundary between low and high-FIP classifications, but models and observations also show different levels of fractionation between different low-FIP or high-FIP element pairs [6]. We see also differences in FIP bias that are dependent on spatial location, such as the differences from footpoint to loop top in post-flare loops [49,52] and sigmoidal ARs [64].

On the stellar evolution arguments, as noted some of the measurements are predicated on the assumption of solar photospheric abundances since stellar photospheric data are not always available, and the evolution of coronal abundances over the solar cycle also implies that any of the stellar data points in Figure 3 could be moving. Nevertheless, we believe that the overarching picture we have described can help to highlight areas that need further investigation in the future.

Acknowledgements. We thank the Royal Society for its support throughout the organization of the Theo Murphy meeting and the production of this special issue. The work of DHB and HPW was supported by the NASA Hinode program. The work of PT was supported by NASA contract NNM07AB07C (Hinode/XRT) to the Smithsonian Astrophysical Observatory, contract 8100002705 (IRIS) to the Smithsonian Astrophysical Observatory, NASA Heliophysics Guest Investigator grant 80NSSC21K0737, and by the NASA Heliophysics Supporting Research grant 80NSSC21K1684. The AIA and EVE data are courtesy of NASA/SDO and the AIA, EVE, and HMI science teams.

References

1. Pottasch SR. 1963 The Lower Solar Corona: Interpretation of the Ultraviolet Spectrum.. *apj* **137**, 945. ([10.1086/147569](https://doi.org/10.1086/147569))
2. Meyer JP. 1985 Solar-stellar outer atmospheres and energetic particles, and galactic cosmic rays. *ApJS* **57**, 173–204. ([10.1086/191001](https://doi.org/10.1086/191001))
3. McIntosh SW, de Pontieu B, Carlsson M, Hansteen V, Boerner P, Goossens M. 2011 Alfvénic waves with sufficient energy to power the quiet solar corona and fast solar wind. *Nature* **475**, 477–480. ([10.1038/nature10235](https://doi.org/10.1038/nature10235))
4. Laming JM. 2004 A Unified Picture of the First Ionization Potential and Inverse First Ionization Potential Effects. *ApJ* **614**, 1063–1072. ([10.1086/423780](https://doi.org/10.1086/423780))
5. Laming JM. 2015 The FIP and Inverse FIP Effects in Solar and Stellar Coronae. *Living Reviews in Solar Physics* **12**, 2. ([10.1007/lrsp-2015-2](https://doi.org/10.1007/lrsp-2015-2))
6. Laming JM, Vourlidis A, Korendyke C, Chua D, Cranmer SR, Ko YK, Kuroda N, Provornikova E, Raymond JC, Raouafi NE, Strachan L, Tun-Beltran S, Weberg M, Wood BE. 2019 Element Abundances: A New Diagnostic for the Solar Wind. *ApJ* **879**, 124. ([10.3847/1538-4357/ab23f1](https://doi.org/10.3847/1538-4357/ab23f1))
7. Mihailescu T, Brooks DH, Laming JM, Baker D, Green LM, James AW, Long DM, van Driel-Gesztelyi L, Stangalini M. 2023 Intriguing Plasma Composition Pattern in a Solar Active Region: A Result of Nonresonant Alfvén Waves?. *ApJ* **959**, 72. ([10.3847/1538-4357/ad05bf](https://doi.org/10.3847/1538-4357/ad05bf))
8. Stangalini M, Baker D, Valori G, Jess DB, Jafarzadeh S, Murabito M, To ASH, Brooks DH, Ermolli I, Giorgi F, MacBride CD. 2021 Spectropolarimetric fluctuations in a sunspot chromosphere. *Philosophical Transactions of the Royal Society of London Series A* **379**, 20200216. ([10.1098/rsta.2020.0216](https://doi.org/10.1098/rsta.2020.0216))
9. Baker D, Stangalini M, Valori G, Brooks DH, To ASH, van Driel-Gesztelyi L, Démoulin P, Stansby D, Jess DB, Jafarzadeh S. 2021 Alfvénic Perturbations in a Sunspot Chromosphere Linked to Fractionated Plasma in the Corona. *ApJ* **907**, 16. ([10.3847/1538-4357/abcafd](https://doi.org/10.3847/1538-4357/abcafd))
10. Murabito M, Stangalini M, Laming JM, Baker D, To ASH, Long DM, Brooks DH, Jafarzadeh S, Jess DB, Valori G. 2024 Observation of Alfvén Wave Reflection in the Solar

- Chromosphere: Ponderomotive Force and First Ionization Potential Effect. *PRL* **132**, 215201. ([10.1103/PhysRevLett.132.215201](https://doi.org/10.1103/PhysRevLett.132.215201))
11. Martínez-Sykora J, De Pontieu B, Hansteen VH, Testa P, Wargnier QM, Szydlarski M. 2023 The Impact of Multifluid Effects in the Solar Chromosphere on the Ponderomotive Force under SE and NEQ Ionization Conditions. *ApJ* **949**, 112. ([10.3847/1538-4357/acc465](https://doi.org/10.3847/1538-4357/acc465))
 12. Doschek GA, Warren HP, Feldman U. 2015 Anomalous Relative Ar/Ca Coronal Abundances Observed by the Hinode/EUV Imaging Spectrometer Near Sunspots. *ApJL* **808**, L7. ([10.1088/2041-8205/808/1/L7](https://doi.org/10.1088/2041-8205/808/1/L7))
 13. Brinkman AC, Behar E, Güdel M, Audard M, den Boggende AJF, Branduardi-Raymont G, Cottam J, Erd C, den Herder JW, Jansen F, Kaastra JS, Kahn SM, Mewe R, Paerels FBS, Peterson JR, Rasmussen AP, Sakelliou I, de Vries C. 2001 First light measurements with the XMM-Newton reflection grating spectrometers: Evidence for an inverse first ionisation potential effect and anomalous Ne abundance in the Coronae of HR 1099. *A&A* **365**, L324–L328. ([10.1051/0004-6361:20000047](https://doi.org/10.1051/0004-6361:20000047))
 14. Drake JJ, Brickhouse NS, Kashyap V, Laming JM, Huenemoerder DP, Smith R, Wargelin BJ. 2001 Enhanced Noble Gases in the Coronae of Active Stars. *ApJL* **548**, L81–L85. ([10.1086/318933](https://doi.org/10.1086/318933))
 15. Güdel M, Audard M, Briggs K, Haberl F, Magee H, Maggio A, Mewe R, Pallavicini R, Pye J. 2001 The XMM-Newton view of stellar coronae: X-ray spectroscopy of the corona of <ASTROBJ>AB Doradus</ASTROBJ>. *A&A* **365**, L336–L343. ([10.1051/0004-6361:20000220](https://doi.org/10.1051/0004-6361:20000220))
 16. Robrade J, Schmitt JHMM. 2005 X-ray properties of active M dwarfs as observed by XMM-Newton. *A&A* **435**, 1073–1085. ([10.1051/0004-6361:20041941](https://doi.org/10.1051/0004-6361:20041941))
 17. Baker D, van Driel-Gesztelyi L, Brooks DH, Valori G, James AW, Laming JM, Long DM, Démoulin P, Green LM, Matthews SA, Oláh K, Kóvári Z. 2019 Transient Inverse-FIP Plasma Composition Evolution within a Solar Flare. *ApJ* **875**, 35. ([10.3847/1538-4357/ab07c1](https://doi.org/10.3847/1538-4357/ab07c1))
 18. Brooks DH, Baker D, van Driel-Gesztelyi L, Warren HP, Yardley SL. 2022 Detection of Stellar-like Abundance Anomalies in the Slow Solar Wind. *ApJL* **930**, L10. ([10.3847/2041-8213/ac6878](https://doi.org/10.3847/2041-8213/ac6878))
 19. Brooks DH. 2018 A Diagnostic of Coronal Elemental Behavior during the Inverse FIP Effect in Solar Flares. *ApJ* **863**, 140. ([10.3847/1538-4357/aad415](https://doi.org/10.3847/1538-4357/aad415))
 20. Doschek GA, Warren HP. 2016 The Mysterious Case of the Solar Argon Abundance near Sunspots in Flares. *ApJ* **825**, 36. ([10.3847/0004-637X/825/1/36](https://doi.org/10.3847/0004-637X/825/1/36))
 21. Peretz U, Behar E, Drake SA. 2015 Coronae of stars with supersolar elemental abundances. *A&A* **577**, A93. ([10.1051/0004-6361/201424769](https://doi.org/10.1051/0004-6361/201424769))
 22. Klimchuk JA. 2006 On Solving the Coronal Heating Problem. *Sol. Phys.* **234**, 41–77. ([10.1007/s11207-006-0055-z](https://doi.org/10.1007/s11207-006-0055-z))
 23. Warren HP, Ugarte-Urra I, Doschek GA, Brooks DH, Williams DR. 2008 Observations of Active Region Loops with the EUV Imaging Spectrometer on Hinode. *ApJL* **686**, L131. ([10.1086/592960](https://doi.org/10.1086/592960))
 24. Brooks DH, Warren HP, Ugarte-Urra I. 2012 Solar Coronal Loops Resolved by Hinode and the Solar Dynamics Observatory. *ApJL* **755**, L33. ([10.1088/2041-8205/755/2/L33](https://doi.org/10.1088/2041-8205/755/2/L33))
 25. Tarr L, Longcope D, Millhouse M. 2013 Calculating Separate Magnetic Free Energy Estimates for Active Regions Producing Multiple Flares: NOAA AR11158. *ApJ* **770**, 4. ([10.1088/0004-637X/770/1/4](https://doi.org/10.1088/0004-637X/770/1/4))
 26. Inoue S, Hayashi K, Shiota D, Magara T, Choe GS. 2013 Magnetic Structure Producing X- and M-class Solar Flares in Solar Active Region 11158. *ApJ* **770**, 79. ([10.1088/0004-637X/770/1/79](https://doi.org/10.1088/0004-637X/770/1/79))
 27. Kay C, Gopalswamy N, Xie H, Yashiro S. 2017 Deflection and Rotation of CMEs from Active Region 11158. *Sol.Phys.* **292**, 78. ([10.1007/s11207-017-1098-z](https://doi.org/10.1007/s11207-017-1098-z))
 28. Norton AA, Stutz RB, Welsch BT. 2021 Oscillations observed in umbra, plage, quiet-Sun and the polarity inversion line of active region 11158 using Helioseismic Magnetic Imager/Solar Dynamics Observatory data. *Philosophical Transactions of the Royal Society of London Series A* **379**, 20200175. ([10.1098/rsta.2020.0175](https://doi.org/10.1098/rsta.2020.0175))
 29. Warren HP, Winebarger AR, Brooks DH. 2012 A Systematic Survey of High-temperature Emission in Solar Active Regions. *ApJ* **759**, 141. ([10.1088/0004-637X/759/2/141](https://doi.org/10.1088/0004-637X/759/2/141))
 30. Watanabe K, Masuda S, Segawa T. 2012 Hinode Flare Catalogue. *Sol. Phys.* **279**, 317–322. ([10.1007/s11207-012-9983-y](https://doi.org/10.1007/s11207-012-9983-y))
 31. Culhane JL, Harra LK, James AM, Al-Janabi K, Bradley LJ, Chaudry RA, Rees K, Tandy JA, Thomas P, Whillock MCR, Winter B, Doschek GA, Korendyke CM, Brown CM, Myers S,

- Mariska J, Seely J, Lang J, Kent BJ, Shaughnessy BM, Young PR, Simnett GM, Castelli CM, Mahmoud S, Mapson-Menard H, Probyn BJ, Thomas RJ, Davila J, Dere K, Windt D, Shea J, Hagood R, Moye R, Hara H, Watanabe T, Matsuzaki K, Kosugi T, Hansteen V, Wikstol Ø. 2007 The EUV Imaging Spectrometer for Hinode. *Sol. Phys.* **243**, 19–61. ([10.1007/s01007-007-0293-1](https://doi.org/10.1007/s01007-007-0293-1))
32. Testa P, De Pontieu B, Allred J, Carlsson M, Reale F, Daw A, Hansteen V, Martinez-Sykora J, Liu W, DeLuca EE, Golub L, McKillop S, Reeves K, Saar S, Tian H, Lemen J, Title A, Boerner P, Hurlburt N, Tarbell TD, Wuelser JP, Kleint L, Kankelborg C, Jaeggli S. 2014 Evidence of nonthermal particles in coronal loops heated impulsively by nanoflares. *Science* **346**, 1255724. ([10.1126/science.1255724](https://doi.org/10.1126/science.1255724))
 33. Testa P, Polito V, De Pontieu B. 2020 IRIS Observations of Short-term Variability in Moss Associated with Transient Hot Coronal Loops. *ApJ* **889**, 124. ([10.3847/1538-4357/ab63cf](https://doi.org/10.3847/1538-4357/ab63cf))
 34. Cho K, Testa P, De Pontieu B, Polito V. 2023 A Statistical Study of IRIS Observational Signatures of Nanoflares and Nonthermal Particles. *ApJ* **945**, 143. ([10.3847/1538-4357/acb7da](https://doi.org/10.3847/1538-4357/acb7da))
 35. Ugarte-Urra I, Warren HP. 2012 Is Active Region Core Variability Age Dependent?. *ApJ* **761**, 21. ([10.1088/0004-637X/761/1/21](https://doi.org/10.1088/0004-637X/761/1/21))
 36. Parker EN. 1988 Nanoflares and the Solar X-Ray Corona. *ApJ* **330**, 474. ([10.1086/166485](https://doi.org/10.1086/166485))
 37. Hood AW, Cargill PJ, Browning PK, Tam KV. 2016 An MHD Avalanche in a Multi-threaded Coronal Loop. *ApJ* **817**, 5. ([10.3847/0004-637X/817/1/5](https://doi.org/10.3847/0004-637X/817/1/5))
 38. Cozzo G, Reid J, Pagano P, Reale F, Hood AW. 2023 Coronal energy release by MHD avalanches. Effects on a structured, active region, multi-threaded coronal loop. *A&A* **678**, A40. ([10.1051/0004-6361/202346689](https://doi.org/10.1051/0004-6361/202346689))
 39. van Ballegoijen AA, Asgari-Targhi M, Cranmer SR, DeLuca EE. 2011 Heating of the Solar Chromosphere and Corona by Alfvén Wave Turbulence. *ApJ* **736**, 3. ([10.1088/0004-637X/736/1/3](https://doi.org/10.1088/0004-637X/736/1/3))
 40. De Pontieu B, McIntosh SW, Hansteen VH, Schrijver CJ. 2009 Observing the Roots of Solar Coronal Heating—in the Chromosphere. *ApJL* **701**, L1–L6. ([10.1088/0004-637X/701/1/L1](https://doi.org/10.1088/0004-637X/701/1/L1))
 41. De Pontieu B, McIntosh SW, Carlsson M, Hansteen VH, Tarbell TD, Boerner P, Martinez-Sykora J, Schrijver CJ, Title AM. 2011 The Origins of Hot Plasma in the Solar Corona. *Science* **331**, 55. ([10.1126/science.1197738](https://doi.org/10.1126/science.1197738))
 42. Martínez-Sykora J, De Pontieu B, Hansteen VH, Rouppe van der Voort L, Carlsson M, Pereira TMD. 2017 On the generation of solar spicules and Alfvénic waves. *Science* **356**, 1269–1272. ([10.1126/science.aah5412](https://doi.org/10.1126/science.aah5412))
 43. Bose S, Joshi J, Testa P, De Pontieu B. 2025 On the Million-degree Signature of Spicules. *ApJL* **983**, L7. ([10.3847/2041-8213/adc30d](https://doi.org/10.3847/2041-8213/adc30d))
 44. Reale F, Testa P, Petralia A, Graham DR. 2019 Impulsive Coronal Heating from Large-scale Magnetic Rearrangements: From IRIS to SDO/AIA. *ApJ* **882**, 7. ([10.3847/1538-4357/ab304f](https://doi.org/10.3847/1538-4357/ab304f))
 45. Testa P, Reale F. 2023 The Solar X-Ray Corona. In *Handbook of X-ray and Gamma-ray Astrophysics*, p. 134. ([10.1007/978-981-16-4544-0_77-1](https://doi.org/10.1007/978-981-16-4544-0_77-1))
 46. Baker D, Brooks DH, van Driel-Gesztelyi L, James AW, Démoulin P, Long DM, Warren HP, Williams DR. 2018 Coronal Elemental Abundances in Solar Emerging Flux Regions. *ApJ* **856**, 71. ([10.3847/1538-4357/aaadb0](https://doi.org/10.3847/1538-4357/aaadb0))
 47. Lanzafame AC, Brooks DH, Lang J. 2005 ADAS analysis of the differential emission measure structure of the inner solar corona. II. A study of the “quiet Sun” inhomogeneities from SOHO CDS-NIS spectra. *A&A* **432**, 1063–1079. ([10.1051/0004-6361:20042113](https://doi.org/10.1051/0004-6361:20042113))
 48. Warren HP. 2014 Measurements of Absolute Abundances in Solar Flares. *ApJL* **786**, L2. ([10.1088/2041-8205/786/1/L2](https://doi.org/10.1088/2041-8205/786/1/L2))
 49. Doschek GA, Warren HP, Harra LK, Culhane JL, Watanabe T, Hara H. 2018 Photospheric and Coronal Abundances in an X8.3 Class Limb Flare. *ApJ* **853**, 178. ([10.3847/1538-4357/aaa4f5](https://doi.org/10.3847/1538-4357/aaa4f5))
 50. Mondal B, Sarkar A, Vadawale SV, Mithun NPS, Janardhan P, Del Zanna G, Mason HE, Mitra-Kraev U, Narendranath S. 2021 Evolution of Elemental Abundances during B-Class Solar Flares: Soft X-Ray Spectral Measurements with Chandrayaan-2 XSM. *ApJ* **920**, 4. ([10.3847/1538-4357/ac14c1](https://doi.org/10.3847/1538-4357/ac14c1))
 51. Rao YK, Mondal B, Del Zanna G, Mithun NPS, Vadawale SV, Reeves KK, Mason HE, Bhardwaj A. 2023 Multiwavelength Observations of a B-class Flare Using XSM, AIA, and XRT. *ApJ* **958**, 190. ([10.3847/1538-4357/acf46a](https://doi.org/10.3847/1538-4357/acf46a))
 52. To ASH, Brooks DH, Imada S, French RJ, van Driel-Gesztelyi L, Baker D, Long DM, Ashfield, IV W, Hayes LA. 2024 Spatially resolved plasma composition evolution in a solar flare – The effect of reconnection outflow. *A&A* **691**, A95. ([10.1051/0004-6361/202449246](https://doi.org/10.1051/0004-6361/202449246))

53. Brooks DH, Ugarte-Urra I, Warren HP. 2008 The Role of Transient Brightenings in Heating the Solar Corona. *ApJL* **689**, L77. ([10.1086/595745](https://doi.org/10.1086/595745))
54. Warren HP, Brooks DH, Doschek GA, Feldman U. 2016 Transition Region Abundance Measurements During Impulsive Heating Events. *ApJ* **824**, 56. ([10.3847/0004-637X/824/1/56](https://doi.org/10.3847/0004-637X/824/1/56))
55. Sakao T, Kano R, Narukage N, Kotoku J, Bando T, DeLuca EE, Lundquist LL, Tsuneta S, Harra LK, Katsukawa Y, Kubo M, Hara H, Matsuzaki K, Shimojo M, Bookbinder JA, Golub L, Korreck KE, Su Y, Shibasaki K, Shimizu T, Nakatani I. 2007 Continuous Plasma Outflows from the Edge of a Solar Active Region as a Possible Source of Solar Wind. *Science* **318**, 1585. ([10.1126/science.1147292](https://doi.org/10.1126/science.1147292))
56. Harra LK, Sakao T, Mandrini CH, Hara H, Imada S, Young PR, van Driel-Gesztelyi L, Baker D. 2008 Outflows at the Edges of Active Regions: Contribution to Solar Wind Formation?. *ApJL* **676**, L147. ([10.1086/587485](https://doi.org/10.1086/587485))
57. Doschek GA, Warren HP, Mariska JT, Muglach K, Culhane JL, Hara H, Watanabe T. 2008 Flows and Nonthermal Velocities in Solar Active Regions Observed with the EUV Imaging Spectrometer on Hinode: A Tracer of Active Region Sources of Heliospheric Magnetic Fields?. *ApJ* **686**, 1362–1371. ([10.1086/591724](https://doi.org/10.1086/591724))
58. Brooks DH, Harra L, Bale SD, Barczynski K, Mandrini C, Polito V, Warren HP. 2021 The Formation and Lifetime of Outflows in a Solar Active Region. *ApJ* **917**, 25. ([10.3847/1538-4357/ac0917](https://doi.org/10.3847/1538-4357/ac0917))
59. Fisk LA. 2003 Acceleration of the solar wind as a result of the reconnection of open magnetic flux with coronal loops. *Journal of Geophysical Research (Space Physics)* **108**, 1157. ([10.1029/2002JA009284](https://doi.org/10.1029/2002JA009284))
60. Crooker NU, Owens MJ. 2012 Interchange Reconnection: Remote Sensing of Solar Signature and Role in Heliospheric Magnetic Flux Budget. *Sp. Sci. Rev.* **172**, 201–208. ([10.1007/s11214-011-9748-1](https://doi.org/10.1007/s11214-011-9748-1))
61. Feldman U, Warren HP, Brown CM, Doschek GA. 2009 Can the Composition of the Solar Corona Be Derived from Hinode/Extreme-Ultraviolet Imaging Spectrometer Spectra?. *ApJ* **695**, 36–45. ([10.1088/0004-637X/695/1/36](https://doi.org/10.1088/0004-637X/695/1/36))
62. Brooks DH, Warren HP. 2011 Establishing a Connection Between Active Region Outflows and the Solar Wind: Abundance Measurements with EIS/Hinode. *ApJL* **727**, L13. ([10.1088/2041-8205/727/1/L13](https://doi.org/10.1088/2041-8205/727/1/L13))
63. Testa P, Martínez-Sykora J, De Pontieu B. 2023 Coronal Abundances in an Active Region: Evolution and Underlying Chromospheric and Transition Region Properties. *ApJ* **944**, 117. ([10.3847/1538-4357/acb343](https://doi.org/10.3847/1538-4357/acb343))
64. Baker D, Brooks DH, Démoulin P, van Driel-Gesztelyi L, Green LM, Steed K, Carlyle J. 2013 Plasma Composition in a Sigmoidal Anemone Active Region. *ApJ* **778**, 69. ([10.1088/0004-637X/778/1/69](https://doi.org/10.1088/0004-637X/778/1/69))
65. Brooks DH, Winebarger AR, Savage S, Warren HP, De Pontieu B, Peter H, Cirtain JW, Golub L, Kobayashi K, McIntosh SW, McKenzie D, Morton R, Rachmeler L, Testa P, Tiwari S, Walsh R. 2020 The Drivers of Active Region Outflows into the Slow Solar Wind. *ApJ* **894**, 144. ([10.3847/1538-4357/ab8a4c](https://doi.org/10.3847/1538-4357/ab8a4c))
66. Young PR, Mason HE. 1997 The Mg/Ne abundance ratio in a recently emerged flux region observed by CDS. *Sol. Phys.* **175**, 523–539. ([10.1023/A:1004936106427](https://doi.org/10.1023/A:1004936106427))
67. Widing KG, Feldman U. 2001 On the Rate of Abundance Modifications versus Time in Active Region Plasmas. *ApJ* **555**, 426–434. ([10.1086/321482](https://doi.org/10.1086/321482))
68. Baker D, Brooks DH, Démoulin P, Yardley SL, van Driel-Gesztelyi L, Long DM, Green LM. 2015 FIP Bias Evolution in a Decaying Active Region. *ApJ* **802**, 104. ([10.1088/0004-637X/802/2/104](https://doi.org/10.1088/0004-637X/802/2/104))
69. Brooks DH, Baker D, van Driel-Gesztelyi L, Warren HP. 2017 A Solar cycle correlation of coronal element abundances in Sun-as-a-star observations. *Nature Communications* **8**, 183. ([10.1038/s41467-017-00328-7](https://doi.org/10.1038/s41467-017-00328-7))
70. Kasper JC, Stevens ML, Lazarus AJ, Steinberg JT, Ogilvie KW. 2007 Solar Wind Helium Abundance as a Function of Speed and Heliographic Latitude: Variation through a Solar Cycle. *ApJ* **660**, 901–910. ([10.1086/510842](https://doi.org/10.1086/510842))
71. McIntosh SW, Kiefer KK, Leamon RJ, Kasper JC, Stevens ML. 2011 Solar Cycle Variations in the Elemental Abundance of Helium and Fractionation of Iron in the Fast Solar Wind: Indicators of an Evolving Energetic Release of Mass from the Lower Solar Atmosphere. *ApJL* **740**, L23. ([10.1088/2041-8205/740/1/L23](https://doi.org/10.1088/2041-8205/740/1/L23))

72. Lepri ST, Landi E, Zurbuchen TH. 2013 Solar Wind Heavy Ions over Solar Cycle 23: ACE/SWICS Measurements. *ApJ* **768**, 94. ([10.1088/0004-637X/768/1/94](https://doi.org/10.1088/0004-637X/768/1/94))
73. Kasper JC, Stevens ML, Korreck KE, Maruca BA, Kiefer KK, Schwadron NA, Lepri ST. 2012 Evolution of the Relationships between Helium Abundance, Minor Ion Charge State, and Solar Wind Speed over the Solar Cycle. *ApJ* **745**, 162. ([10.1088/0004-637X/745/2/162](https://doi.org/10.1088/0004-637X/745/2/162))
74. Shearer P, von Steiger R, Raines JM, Lepri ST, Thomas JW, Gilbert JA, Landi E, Zurbuchen TH. 2014 The Solar Wind Neon Abundance Observed with ACE/SWICS and Ulysses/SWICS. *ApJ* **789**, 60. ([10.1088/0004-637X/789/1/60](https://doi.org/10.1088/0004-637X/789/1/60))
75. Landi E, Testa P. 2015 Neon and Oxygen Abundances and Abundance Ratio in the Solar Corona. *ApJ* **800**, 110. ([10.1088/0004-637X/800/2/110](https://doi.org/10.1088/0004-637X/800/2/110))
76. Ko YK, Young PR, Muglach K, Warren HP, Ugarte-Urra I. 2016 Correlation of Coronal Plasma Properties and Solar Magnetic Field in a Decaying Active Region. *ApJ* **826**, 126. ([10.3847/0004-637X/826/2/126](https://doi.org/10.3847/0004-637X/826/2/126))
77. Brooks DH, Ugarte-Urra I, Warren HP. 2015 Full-Sun observations for identifying the source of the slow solar wind. *Nature Communications* **6**, 5947. ([10.1038/ncomms6947](https://doi.org/10.1038/ncomms6947))
78. Brooks DH, Warren HP, Williams DR, Watanabe T. 2009 Hinode/Extreme-Ultraviolet Imaging Spectrometer Observations of the Temperature Structure of the Quiet Corona. *ApJ* **705**, 1522–1532. ([10.1088/0004-637X/705/2/1522](https://doi.org/10.1088/0004-637X/705/2/1522))
79. To ASH, James AW, Bastian TS, van Driel-Gesztelyi L, Long DM, Baker D, Brooks DH, Lomuscio S, Stansby D, Valori G. 2023 Understanding the Relationship between Solar Coronal Abundances and F10.7 cm Radio Emission. *ApJ* **948**, 121. ([10.3847/1538-4357/acbc1b](https://doi.org/10.3847/1538-4357/acbc1b))
80. Wood BE, Linsky JL. 2010 Resolving the ξ Boo Binary with Chandra, and Revealing the Spectral Type Dependence of the Coronal “FIP Effect”. *ApJ* **717**, 1279–1290. ([10.1088/0004-637X/717/2/1279](https://doi.org/10.1088/0004-637X/717/2/1279))
81. Testa P, Saar SH, Drake JJ. 2015 Stellar activity and coronal heating: an overview of recent results. *Philosophical Transactions of the Royal Society of London Series A* **373**, 20140259–20140259. ([10.1098/rsta.2014.0259](https://doi.org/10.1098/rsta.2014.0259))
82. Seli B, Oláh K, Kriskovics L, Kővári Z, Vida K, Balázs LG, Laming JM, van Driel-Gesztelyi L, Baker D. 2022 Extending the FIP bias sample to magnetically active stars. Challenging the FIP bias paradigm. *A&A* **659**, A3. ([10.1051/0004-6361/202141493](https://doi.org/10.1051/0004-6361/202141493))
83. Asplund M, Grevesse N, Sauval AJ, Scott P. 2009 The Chemical Composition of the Sun. *Ann.Rev.A&A* **47**, 481–522. ([10.1146/annurev.astro.46.060407.145222](https://doi.org/10.1146/annurev.astro.46.060407.145222))
84. Drake JJ, Testa P. 2005 The ‘solar model problem’ solved by the abundance of neon in nearby stars. *Nature* **436**, 525–528. ([10.1038/nature03803](https://doi.org/10.1038/nature03803))
85. Telleschi A, Güdel M, Briggs K, Audard M, Ness JU, Skinner SL. 2005 Coronal Evolution of the Sun in Time: High-Resolution X-Ray Spectroscopy of Solar Analogs with Different Ages. *ApJ* **622**, 653–679. ([10.1086/428109](https://doi.org/10.1086/428109))
86. Baker D, van Driel-Gesztelyi L, James AW, Démoulin P, To ASH, Murabito M, Long DM, Brooks DH, McKeivitt J, Laming JM, Green LM, Yardley SL, Valori G, Mihailescu T, Matthews SA, Kuniyoshi H. 2024 Searching for Evidence of Subchromospheric Magnetic Reconnection on the Sun. *ApJ* **970**, 39. ([10.3847/1538-4357/ad4a6e](https://doi.org/10.3847/1538-4357/ad4a6e))
87. Drake JJ, Laming JM, Widing KG, Schmitt JHMM, Haisch B, Bowyer S. 1995 The Elemental Composition of the Corona of Procyon: Evidence for the Absence of the FIP Effect. *Science* **267**, 1470–1473. ([10.1126/science.267.5203.1470](https://doi.org/10.1126/science.267.5203.1470))
88. Craig IJD, Brown JC. 1976 Fundamental limitations of X-ray spectra as diagnostics of plasma temperature structure.. *A&A* **49**, 239–250.
89. Judge PG, Hubeny V, Brown JC. 1997 Fundamental Limitations of Emission-Line Spectra as Diagnostics of Plasma Temperature and Density Structure. *ApJ* **475**, 275–290. ([10.1086/303511](https://doi.org/10.1086/303511))
90. Testa P, De Pontieu B, Martínez-Sykora J, Hansteen V, Carlsson M. 2012 Investigating the Reliability of Coronal Emission Measure Distribution Diagnostics using Three-dimensional Radiative Magnetohydrodynamic Simulations. *ApJ* **758**, 54. ([10.1088/0004-637X/758/1/54](https://doi.org/10.1088/0004-637X/758/1/54))